



Multi-parameters optimization for microchannel heat sink using inverse problem method

Zheng-Hua Wang^a, Xiao-Dong Wang^{a,*}, Wei-Mon Yan^{b,*}, Yuan-Yuan Duan^c, Duu-Jong Lee^d, Jin-Liang Xu^a

^a Beijing Key Laboratory of New and Renewable Energy, North China Electric Power University, Beijing 102206, China

^b Department of Greenery, National University of Tainan, Tainan 70005, Taiwan

^c Key Laboratory for Thermal Science and Power Engineering of MOE, Tsinghua University, Beijing 100084, China

^d Department of Chemical Engineering, College of Engineering, National Taiwan University of Science and Technology, Taipei 106, Taiwan

ARTICLE INFO

Article history:

Received 26 June 2010

Received in revised form 27 January 2011

Accepted 27 January 2011

Available online 5 April 2011

Keywords:

Micro-channel

Heat sink

Optimization

Inverse geometry design

ABSTRACT

This work describes an inverse problem method to optimize the geometric design for microchannel heat sinks using a novel multi-parameter optimization approach, which integrates the simplified conjugate-gradient scheme and a fully developing three-dimensional heat transfer and flow model. Overall thermal resistance is the objective function to be minimized with number of channels, N , channel aspect ratio, α , and the ratio of channel width to pitch, β , as search variables. With a constant bottom area ($10 \text{ mm} \times 10 \text{ mm}$), constant heat flux applied to the heat sink bottom surface (100 W cm^{-2}), and constant pumping power (0.05 W), the optimal design values are $N = 71$, $\alpha = 8.24$, and $\beta = 0.6$, with a minimum overall thermal resistance of 0.144 K W^{-1} . Increasing pumping power reduces overall thermal resistance of the optimal design; however, the design's effectiveness declines significantly under high pumping power. The N and α values in the optimal design increase and β decreases as pumping power increases.

© 2011 Elsevier Ltd. All rights reserved.

1. Introduction

Microchannel heat sink first proposed by Tuckerman and Pease [1] has advantages over conventional heat sink such as higher heat dissipation, smaller size and volume per heat load, lower coolant requirement and lower operational cost, etc. The microchannel heat sink has become an important cooling device to very-large-scale integrated (VLSI) circuits and Micro-Electro Mechanical System (MEMS) applications [2–5].

Many experimental [1,6–9] and numerical [2–5,10–31] studies were conducted to investigate the performance of microchannel heat sink as a function of solid materials, coolant fluids and channel dimensions. Simplified fin models and two-dimensional models were used in early stage to determine thermal resistance of microchannel heat sink [10–14]. Later, three-dimensional models were developed, conjugating solid-coolant heat transfer and assuming fully developed flow and thermal fields, to analyze the heat transfer characteristics of microchannel heat sink [2–5,15–28]. Toh et al. [29] numerically computed the three-dimensional fluid flow and heat transfer rate at the entrance regime of a microchannel heat sink. Al-Bakhit and Fakheri [30] noted that the relatively short length and relatively thick channel wall preclude the

possible existence of fully developed fluid and thermal fields in microchannel heat exchangers. Restated, three-dimensional heat transfer model considering effects of entrance regime should be developed for microchannel heat exchanger simulation.

Optimal structure for microchannel heat sink was searched for using the “direct problem solve” approach [23–27]. Kim [23] adopted the fin model, the porous model, and the numerical optimization method to explore the minimum overall thermal resistance for a heat sink at pumping power at 2.56 W . Ambatipudi and Rahman [24] performed numerical simulations for conjugated heat transfer process in microchannel heat sink at varying channel depth, channel width, number of channel and flow rate. These authors noted that performance of the heat sink can be enhanced by increasing the number of channels and the through-channel flow rate. Li and Peterson [25,26] developed a semi-normalized three-dimensional heat transfer model and carried out numerical optimization for minimizing thermal resistance. Under a constant pumping power of 0.05 W , the optimal geometric configuration determined by Li and Peterson model has 100 channels with width of $60 \mu\text{m}$ and height of about $700 \mu\text{m}$. Bello-Ochende et al. [27] presented the scale analysis and the intersection of the asymptotes method to estimate the optimum aspect ratio and channel shape that maximized optimal thermal conductance of a heat sink.

Inverse problem solve method was also used to optimize geometric structure of microchannel heat sink [3,4,28]. Ryu et al. [3] solved transport equations with directional optimization search to minimize thermal resistance of a heat sink at a fixed channel as-

* Corresponding authors. Tel./fax: +86 10 62321277 (X.-D. Wang), tel.: +886 6 2602251; fax: +886 6 2602205 (W.-M. Yan).

E-mail addresses: wangxd99@gmail.com (X.-D. Wang), wmyan@mail.nutn.edu.tw (W.-M. Yan).

Nomenclature

A	base area of the heat sink (m^2)	T_{\max}	maximum temperatures observed in the heat sink (K)
A_c	cross-sectional area of channel (m^2)	T_{\min}	minimum temperatures observed in the heat sink (K)
A_1	convective heat transfer area (m^2)	u, v, w	velocity component in x -, y -, z -directions (m s^{-1})
A_2	heat conduction area (m^2)	u_{in}	inlet velocity of coolant (m s^{-1})
c_1	specific heat of the coolant ($\text{J kg}^{-1} \text{K}^{-1}$)	u_m	average velocity of coolant over channel cross-section (m s^{-1})
C_1, C_2, C_3	the constants in Eq. (17)	\dot{V}	total volumetric flow rate ($\text{m}^3 \text{s}^{-1}$)
D	hydraulic diameter of channel (m)	W_c	channel width (m)
f	Fanning friction factor	W_p	pitch width (m)
h	convective heat transfer coefficient ($\text{W m}^{-2} \text{K}^{-1}$)	W_r	rib width (m)
H_c	channel height (m)		
J	objective function	Greek	
k_1	thermal conductivity of the coolant ($\text{W m}^{-1} \text{K}^{-1}$)	α	aspect ratio of the channel
k_s	thermal conductivity of the solid material ($\text{W m}^{-1} \text{K}^{-1}$)	β	width ratio of channel to pitch
L	mean heat conduction path (m)	$\gamma_N^{(k)}, \gamma_\alpha^{(k)}, \gamma_\beta^{(k)}$	conjugate gradient coefficients of (N, α, β) in the k th search step
L_x	channel length (m)	δ_1	thickness of bottom wall of solid (m)
L_y	height of heat sink (m)	δ_2	thickness of top wall of solid (m)
L_z	width of heat sink (m)	Δp	pressure drop across individual channel (Pa)
N	channel number	μ_l	coolant viscosity ($\text{kg m}^{-1} \text{s}^{-1}$)
p	coolant pressure (Pa)	$\zeta_N^{(k)}, \zeta_\alpha^{(k)}, \zeta_\beta^{(k)}$	search direction of (N, α, β) in the k th search step
p_{in}	inlet pressure of coolant (Pa)	ρ_1	coolant density (kg m^{-3})
p_{out}	outlet pressure of coolant (Pa)	$\chi_N^{(k)}, \chi_\alpha^{(k)}, \chi_\beta^{(k)}$	search step size of (N, α, β) in the k th search step
Pr	Prandtl number	Ω	optimal thermal resistance ($\text{K W}^{-1} \text{m}^{-2}$)
q_w	heat flux applied to bottom surface of heat sink (W m^{-2})		
Re	Reynolds number	Subscripts	
R_T	optimal thermal resistance (K W^{-1})	l	liquid phase
$R_{T,\text{cond}}$	conductive thermal resistance (K W^{-1})	s	solid phase
$R_{T,\text{conv}}$	convective thermal resistance (K W^{-1})		
T_l	coolant temperature (K)		
T_{in}	inlet temperature of coolant (K)		

pect ratio. Kou et al. [4,28] presented a three-dimensional numerical study to search for optimal channel width and height so to reach minimum thermal resistance.

All geometric parameters affect microchannel heat sink performance. To our best knowledge, no study is presented on simultaneous optimization of numerous design parameters including channel number, channel width, and channel height to achieve minimum heat transfer resistance. This work proposed an optimization approach combining the simplified conjugate-gradient method and a fully three-dimensional microchannel heat sink model to look for optimal geometric design considering the minimum overall thermal resistance as the objective function. Three geometric parameters, the channel number, N , the channel aspect ratio, α , and the width ratio of channel to pitch, β , are optimized simultaneously to archive minimum optimal thermal resistance.

2. Geometry for microchannel heat sink

Fig. 1(a) and (b) shows the schematics of the microchannel heat sink and its symmetric unit composed of a channel and two half-ribs investigated herein. The heat sink is fabricated by binding two silicon wafers and each wafer has thickness $L_y/2 = 450 \mu\text{m}$ with the length $L_x = 10 \text{ mm}$ and width $L_z = 10 \text{ mm}$. The heat sink composes of N channels and N ribs with rectangular cross-section. With consideration of practical fabrication technique, the thickness of the bottom wall of the channel, δ_1 , is fixed as $100 \mu\text{m}$; the height of the channel, H_c , is variable, and the thickness of the top wall of the channel, δ_2 , $=L_y - H_c$ is larger than $100 \mu\text{m}$. The channel width W_c and the rib width W_r make the pitch width $W_p = W_c + W_r = L_x/N$. The bottom of the heat sink is attached to a heating surface such as integrated circuits or electronic chips with a uniform heat flux, q_w . The pumping power, Ω , is defined as:

$$\Omega = \dot{V} \Delta p = Nu_m A_c \Delta p \quad (1)$$

where \dot{V} is the total volumetric flow rate, u_m is the average velocity in the channel, $A_c = H_c W_c$ is the cross-sectional area of the channel, and Δp is the pressure drop across the channel. The performance of microchannel heat sink can be evaluated using the optimal thermal resistance, R_T , defined as follows:

$$R_T = \frac{T_{\max} - T_{\min}}{q_w A} = \frac{T_{\max} - T_{l,\text{in}}}{q_w L_x L_z} \quad (2)$$

where T_{\max} and T_{\min} are the maximum and minimum temperatures observed in the heat sink, so T_{\min} is equal to the inlet temperature of the coolant, T_{in} . $A = L_x \times L_z$ is the base area of the heat sink.

3. Optimization method

3.1. Microchannel heat sink model

The computational domain is shown in Fig. 1(b). The following assumptions are made: (1) steady state; (2) single phase and laminar flow; (3) constant fluid and solid properties; (4) negligible gravitational force (4) negligible radiation heat transfer; (5) negligible contract resistance at the interfaces between the solid wall and the coolant. The present model is different from previous studies [4,25,26,28] which assumed thermally and hydraulically fully developed fields. Ryu et al. [3] noted that the thermal entrance effects should not be neglected when the working fluid is water ($Pr \approx 7$). If neglected, this effect would result in a significant error for the averaged Nusselt number (15% for Ryu's simulation case).

Based on the above assumptions, the governing equations for the coolant are listed in the following.

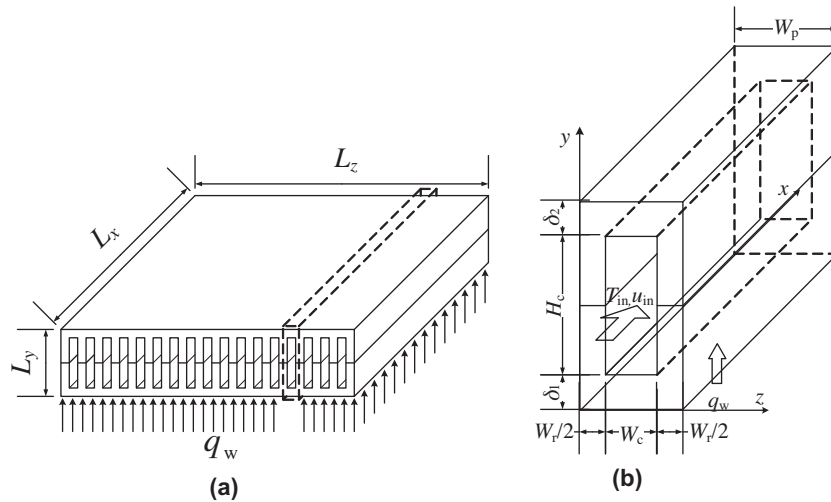


Fig. 1. Schematics of microchannel heat sink: (a) microchannel heat sink and (b) symmetric unit.

Continuity equation for the coolant:

$$\frac{\partial u}{\partial x} + \frac{\partial v}{\partial y} + \frac{\partial w}{\partial z} = 0 \quad (3)$$

where u , v and w are velocity component in x , y and z directions.

Momentum equation for the coolant:

$$\rho_l \left(u \frac{\partial u}{\partial x} + v \frac{\partial u}{\partial y} + w \frac{\partial u}{\partial z} \right) = -\frac{\partial p}{\partial x} + \mu_l \left(\frac{\partial^2 u}{\partial x^2} + \frac{\partial^2 u}{\partial y^2} + \frac{\partial^2 u}{\partial z^2} \right) \quad (4a)$$

$$\rho_l \left(u \frac{\partial v}{\partial x} + v \frac{\partial v}{\partial y} + w \frac{\partial v}{\partial z} \right) = -\frac{\partial p}{\partial y} + \mu_l \left(\frac{\partial^2 v}{\partial x^2} + \frac{\partial^2 v}{\partial y^2} + \frac{\partial^2 v}{\partial z^2} \right) \quad (4b)$$

$$\rho_l \left(u \frac{\partial w}{\partial x} + v \frac{\partial w}{\partial y} + w \frac{\partial w}{\partial z} \right) = -\frac{\partial p}{\partial z} + \mu_l \left(\frac{\partial^2 w}{\partial x^2} + \frac{\partial^2 w}{\partial y^2} + \frac{\partial^2 w}{\partial z^2} \right) \quad (4c)$$

where ρ_l and μ_l are the density and dynamic viscosity of the coolant, and p is the coolant pressure.

Energy equation for the coolant:

$$\rho_l c_l \left(u \frac{\partial T_l}{\partial x} + v \frac{\partial T_l}{\partial y} + w \frac{\partial T_l}{\partial z} \right) = k_l \left(\frac{\partial^2 T_l}{\partial x^2} + \frac{\partial^2 T_l}{\partial y^2} + \frac{\partial^2 T_l}{\partial z^2} \right) \quad (5)$$

where T_l is the coolant temperature, c_l is the specific heat of the coolant, k_l is the thermal conductivity of the coolant.

Energy equation for solid region:

$$0 = k_s \left(\frac{\partial^2 T_s}{\partial x^2} + \frac{\partial^2 T_s}{\partial y^2} + \frac{\partial^2 T_s}{\partial z^2} \right) \quad (6)$$

where T_s is the solid temperature, and k_s is the thermal conductivity of the solid.

The boundary conditions for the governing equations are given as follows.

Inlet:

$$u = u_{in}, \quad v = 0, \quad w = 0, \quad T = T_{in} \quad (7a)$$

Outlet:

$$p = p_{out} \quad (7b)$$

Coolant-solid interface:

$$u = v = w = 0, \quad T_l = T_s, \quad -k_l \frac{\partial T_l}{\partial n} = -k_s \frac{\partial T_s}{\partial n} \quad (7c)$$

Bottom wall of the heat sink:

$$q_w = -k_s \frac{\partial T_s}{\partial n} \quad (7d)$$

Other solid walls and symmetric interface

$$0 = \frac{\partial T_s}{\partial n} \quad (7e)$$

Eq. (7e) assumes no heat loss from solid surface to ambient, which is also adopted in other works [4,25,26,28].

To compare the performance of the heat sinks with various geometric parameters and at the same pumping power, the inlet velocity of the coolant, u_{in} , should be calculated with the given pumping power. Knight [13] proposed that for a fully developed laminar flow, the product of Reynolds number, Re , and Fanning friction factor, f , is dependent on geometric parameters of the channel as follows:

$$\begin{aligned} Ref &= \left(\frac{\rho_l u_m D}{\mu_l} \right) \left(\frac{D}{2\rho_l u_m^2} \frac{p_{in} - p_{out}}{L_x} \right) \\ &= 4.70 + 19.64 \frac{H_c^2 + W_c^2}{(H_c + W_c)^2} = 4.70 + 19.64 \frac{1 + \alpha^2}{(1 + \alpha)^2} \end{aligned} \quad (8)$$

where u_m is the average velocity over cross-section of the channel, $D = 2H_c W_c / (H_c + W_c)$ is the hydraulic diameter, $\alpha = H_c / W_c$ is the aspect ratio of the channel. Thus, once the pumping power, Ω , is given, the inlet velocity and pressure are calculated from Eqs. (1) and (8):

$$u_m = \left(\frac{4\alpha}{2\mu_l (4.70(1 + \alpha)^2 + 19.64(1 + \alpha^2))} \frac{\Omega}{NL_x} \right)^{0.5} \quad (9a)$$

$$\Delta p = p_{in} - p_{out} = \frac{\Omega}{NH_c W_c u_m} \quad (9b)$$

Though Eqs. (8) and (9) hold only for fully developed laminar flow, but u_m is assumed to be equal u_{in} in the present three-dimensional model. We justify this approximation in later sections.

3.2. Simplified conjugate-gradient method

In order to find the optimal performance of the microchannel heat sink, the optimal thermal resistance, R_T , is chosen as the objective function, or

$$J = R_T \quad (10)$$

With a specified A , q_w and Ω as constraints, the performance of heat sink is closely related to its geometric parameters: the number of the channel, N , the aspect ratio of the channel, $\alpha = H_c / W_c$, and the width ratio of the channel to the pitch, $\beta = W_c / (W_c + W_p)$. In the pres-

ent work, all three parameters will be optimized simultaneously. Thus, the objective function can be expressed as:

$$J = R_T(N, \alpha, \beta) \tag{11}$$

where N, α, β are referred to as search variables or design variables, so optimal set of geometric parameters (N, α, β) is searched for to reach the minimum of the optimal thermal resistance.

The conjugate-gradient method evaluates the gradients of the objective function and establishes a conjugate direction for the updated search variables with the help of sensitivity analysis. The negative gradient direction of the objective function is specified as the first search direction in conjugate gradient method; that is,

$$\nabla J = \left(-\frac{\partial R_T}{\partial N}, -\frac{\partial R_T}{\partial \alpha}, -\frac{\partial R_T}{\partial \beta} \right) \tag{12}$$

where $(\partial R_T/\partial N, \partial R_T/\partial \alpha, \partial R_T/\partial \beta)$ are sensitivity coefficients. The sensitivity coefficients are derived by introducing a small perturbation $(\Delta N, \Delta \alpha, \Delta \beta)$ into search variables $(N, \alpha, \text{ and } \beta)$. The new search variables, $(N^{(k+1)}, \alpha^{(k+1)}, \text{ and } \beta^{(k+1)})$, are then updated by

$$\begin{aligned} N^{(k+1)} &= N^{(k)} + \chi_N^{(k)} \zeta_N^{(k+1)} \\ \alpha^{(k+1)} &= \alpha^{(k)} + \chi_\alpha^{(k)} \zeta_\alpha^{(k+1)} \\ \beta^{(k+1)} &= \beta^{(k)} + \chi_\beta^{(k)} \zeta_\beta^{(k+1)} \end{aligned} \tag{13}$$

where $(N^{(k)}, \alpha^{(k)}, \text{ and } \beta^{(k)})$ and $(N^{(k+1)}, \alpha^{(k+1)}, \text{ and } \beta^{(k+1)})$ are the values of $(N, \alpha, \text{ and } \beta)$ in the k th and $(k + 1)$ th search steps, respectively; $(\chi_N^{(k)}, \chi_\alpha^{(k)}, \text{ and } \chi_\beta^{(k)})$ is the search step size of $(N, \alpha, \text{ and } \beta)$ in the k th search step; $(\zeta_N^{(k+1)}, \zeta_\alpha^{(k+1)}, \text{ and } \zeta_\beta^{(k+1)})$ is the search direction of $(N, \alpha, \text{ and } \beta)$, which can be expressed as a linear combination of the previous search direction, $(\zeta_N^{(k)}, \zeta_\alpha^{(k)}, \text{ and } \zeta_\beta^{(k)})$ and the negative gradient direction of the new objective function, $(-\partial R_T/\partial N)^{(k+1)}, -(\partial R_T/\partial \alpha)^{(k+1)}, \text{ and } -(\partial R_T/\partial \beta)^{(k+1)}$; that is,

$$\begin{aligned} \zeta_N^{(k+1)} &= -\frac{\partial R_T^{(k+1)}}{\partial N} + \gamma_N^{(k+1)} \zeta_N^{(k)} \\ \zeta_\alpha^{(k+1)} &= -\frac{\partial R_T^{(k+1)}}{\partial \alpha} + \gamma_\alpha^{(k+1)} \zeta_\alpha^{(k)} \\ \zeta_\beta^{(k+1)} &= -\frac{\partial R_T^{(k+1)}}{\partial \beta} + \gamma_\beta^{(k+1)} \zeta_\beta^{(k)} \end{aligned} \tag{14}$$

where $(\gamma_N^{(k+1)}, \gamma_\alpha^{(k+1)}, \text{ and } \gamma_\beta^{(k+1)})$ are the conjugate gradient coefficients, which must guarantee that $(\zeta_N^{(k)}, \zeta_\alpha^{(k)}, \text{ and } \zeta_\beta^{(k)})$ is conjugated to $(-\partial R_T^{(k+1)}/\partial N, -\partial R_T^{(k+1)}/\partial \alpha, \text{ and } -\partial R_T^{(k+1)}/\partial \beta)$ and expressed as

$$\begin{aligned} \gamma_N^{(k+1)} &= \left(\frac{\partial R_T^{(k+1)}}{\partial N} \middle/ \frac{\partial R_T^{(k)}}{\partial N} \right)^2 \\ \gamma_\alpha^{(k+1)} &= \left(\frac{\partial R_T^{(k+1)}}{\partial \alpha} \middle/ \frac{\partial R_T^{(k)}}{\partial \alpha} \right)^2 \\ \gamma_\beta^{(k+1)} &= \left(\frac{\partial R_T^{(k+1)}}{\partial \beta} \middle/ \frac{\partial R_T^{(k)}}{\partial \beta} \right)^2 \end{aligned} \tag{15}$$

In the conventional conjugate-gradient scheme, optimal search step size, $(\chi_N^{(k)}, \chi_\alpha^{(k)}, \text{ and } \chi_\beta^{(k)})$, must be determined. After the $(k - 1)$ th search, the objective function becomes

$$\begin{aligned} J^{(k)} &= R_T(N^{(k)}, \alpha^{(k)}, \beta^{(k)}) \\ &= R_T\left(N^{(k-1)} + \chi_N^{(k-1)} \zeta_N^{(k)}, \alpha^{(k-1)} + \chi_\alpha^{(k-1)} \zeta_\alpha^{(k)}, \beta^{(k-1)} + \chi_\beta^{(k-1)} \zeta_\beta^{(k)}\right) \end{aligned} \tag{16}$$

The value of $(\chi_N^{(k)}, \chi_\alpha^{(k)}, \text{ and } \chi_\beta^{(k)})$ can be acquired by implementing a one-dimensional search with respect to $(\chi_N^{(k-1)}, \chi_\alpha^{(k-1)}, \text{ and } \chi_\beta^{(k-1)})$ along the negative gradient direction of the objective function under the condition that other search variables remain unchanged. Therefore, when the objective function reaches a minimum in

one-dimensional search procedures, the corresponding value of $(\chi_N^{(k)}, \chi_\alpha^{(k)}, \text{ and } \chi_\beta^{(k)})$ is the optimal search size of $(\chi_N, \chi_\alpha, \text{ and } \chi_\beta)$ in the k th search step. Determining the optimal search step size with the conventional conjugated-gradient procedure is a complex process. In the simplified conjugated-gradient approach, the values of step size $(\chi_N, \chi_\alpha, \text{ and } \chi_\beta)$ are fixed at a constant value without convergence loss [31]; that is,

$$\chi_N = C_1, \quad \chi_\alpha = C_2, \quad \chi_\beta = C_3 \tag{17}$$

The magnitude of $(C_1, C_2, \text{ and } C_3)$ typically differs when each search variable is dependent upon its sensitivity to the objective function. Notably, the convergence speed of iterations during the optimization process often slows with a fixed step size; however, the need to determine the one-dimensional search of step size for each $(\chi_N, \chi_\alpha, \text{ and } \chi_\beta)$ no longer exists.

3.3. Optimization scheme

The initial value of each search variable is first approximated, and the conjugate-gradient coefficients and search directions are analyzed in successive steps to estimate the values of new search variables. This process repeated to obtain the minimum objective function. Specifically, the search procedures are as follows.

- (a) Initially approximate the values of search variables $(N^{(1)}, \alpha^{(1)}, \text{ and } \beta^{(1)})$, and assign these values to step sizes $(\chi_N, \chi_\alpha, \text{ and } \chi_\beta)$.
- (b) Create the geometry and grids of the microchannel heat sink model for the assigned $(N^{(1)}, \alpha^{(1)}, \text{ and } \beta^{(1)})$. Based on a specified constant pumping power, calculate the inlet velocity using Eq. (9a). Specify all boundary conditions, and then numerically solve Eqs. (3)–(5).
- (c) Calculate the objective function $R_T(N^{(1)}, \alpha^{(1)}, \text{ and } \beta^{(1)})$ using Eq. (2). If the convergence criterion is met, terminate iterations; otherwise, proceed to step (d).
- (d) Calculate the sensitivity coefficients, $\left(\frac{\partial R_T^{(k+1)}}{\partial N}, \frac{\partial R_T^{(k+1)}}{\partial \alpha}, \text{ and } \frac{\partial R_T^{(k+1)}}{\partial \beta}\right)$, of the objective function for each search variable, for which (3)–(5) are employed three times to obtain $R_T(N^{(k)} + \Delta N, \alpha^{(k)}, \text{ and } \beta^{(k)})$, $R_T(N^{(k)}, \alpha^{(k)} + \Delta \alpha, \text{ and } \beta^{(k)})$, and $R_T(N^{(k)}, \alpha^{(k)}, \text{ and } \beta^{(k)} + \Delta \beta)$, thus;

$$\begin{aligned} \frac{\partial R_T^{(k+1)}}{\partial N} &= \frac{R_T(N^{(k)} + \Delta N, \alpha^{(k)}, \beta^{(k)}) - R_T(N^{(k)}, \alpha^{(k)}, \beta^{(k)})}{\Delta N} \\ \frac{\partial R_T^{(k+1)}}{\partial \alpha} &= \frac{R_T(N^{(k)}, \alpha^{(k)} + \Delta \alpha, \beta^{(k)}) - R_T(N^{(k)}, \alpha^{(k)}, \beta^{(k)})}{\Delta \alpha} \\ \frac{\partial R_T^{(k+1)}}{\partial \beta} &= \frac{R_T(N^{(k)}, \alpha^{(k)}, \beta^{(k)} + \Delta \beta) - R_T(N^{(k)}, \alpha^{(k)}, \beta^{(k)})}{\Delta \beta} \end{aligned} \tag{18}$$

- (e) Calculate the conjugate-gradient coefficients $(\gamma_N^{(k+1)}, \gamma_\alpha^{(k+1)}, \gamma_\beta^{(k+1)})$ for each search variable using Eq. (15). For the first step with $k = 1$, $(\gamma_N^{(2)}, \gamma_\alpha^{(2)}, \text{ and } \gamma_\beta^{(2)}) = (0, 0, 0)$.
- (f) Calculate the search directions, $(\zeta_N^{(k+1)}, \zeta_\alpha^{(k+1)}, \text{ and } \zeta_\beta^{(k+1)})$, for each search variable using Eq. (14).
- (g) Update new search variables using Eq. (13), and then return to step (b).

In steps (b) and (d), Eqs. (3)–(5) were transformed into a finite-difference form using the control volume method and were solved iteratively with an iteration criterion for convergence of 10^{-6} . Preliminary numerical tests were performed to ensure that the solution is independent of adopted grid size.

4. Results and discussion

4.1. Model validation

Fig. 2 compares the pressure drops predicted by the proposed model and those calculated by Eq. (9b), indicating that satisfactory agreement exists between these two drops. Thus, Eq. (9a) was utilized to calculate u_m in this study.

Table 1 compares predicted results from the proposed model and experimental data [1] using the same dimensions and operating conditions. Under various channel dimensions and operating conditions, the predictions by the proposed model agree with experimental data with a difference of <3.6%.

4.2. Effect of individual parameters

The heat sink solid region is made of silicon with $k_s = 148 \text{ W m}^{-1} \text{ K}^{-1}$. Pure water is the coolant with $k_l = 0.613 \text{ W m}^{-1} \text{ K}^{-1}$, $\mu_l = 0.000855 \text{ kg m}^{-1} \text{ s}^{-1}$, $\rho_l = 997 \text{ kg m}^{-3}$, $c_l = 4179 \text{ J kg}^{-1} \text{ K}^{-1}$ and $T_{in} = 293 \text{ K}$. Uniform heat flux of $q_w = 100 \text{ W cm}^{-2}$ is employed to the heat sink bottom surface with a constant pumping power of $\Omega = 0.05 \text{ W}$.

Before simultaneous optimization of all three parameters, a calculation is performed to examine the effect of individual parameters on heat sink performance. The thicknesses of the top and bottom walls are taken as the same ($\delta_1 = \delta_2 = 100 \mu\text{m}$), and heat sink thickness, L_y , can exceed $900 \mu\text{m}$ to obtain a high α . Fig. 3(a)–(c) shows the effects of number of channels, channel aspect ratios, and ratio of channel width to pitch on optimal thermal resistance of a heat sink. When heat $Q = q_w A = q_w L_x L_z$ was transported from the base surface to the heat sink via heat conduction

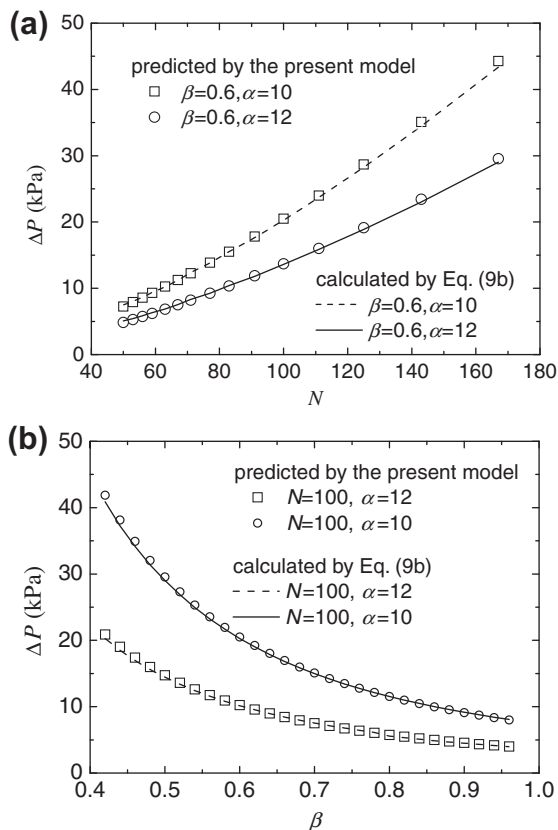


Fig. 2. Comparison of pressure drop between predicted by the present three-dimensional model and calculated by Eq. (9b).

Table 1

Comparison of thermal resistance for various channel dimensions and operating conditions.

	W_r (μm)	W_c (μm)	H_c (μm)	Δp (kPa)	R_T (K W^{-1})	
					Experimental data [1]	Predicted results
1	56	44	320	103.4	0.110	0.110
2	55	45	287	117.2	0.113	0.109
3	50	50	302	213.7	0.090	0.087

through the solid, heat then passes from the solid (microchannel wall) to the coolant (Fig. 4). Overall, thermal resistance can be divided into the following two parts:

$$R_T = R_{T,\text{conv}} + R_{T,\text{cond}} = \frac{1}{hA_1} + \frac{L}{k_s A_2} \quad (19)$$

where $R_{T,\text{conv}}$ and $R_{T,\text{cond}}$ are convective and conductive thermal resistance, respectively; h is the convective heat transfer coefficient, which is closely related to average flow velocity of the coolant over the channel cross section; A_1 is convective heat transfer area for a heat sink with N channels, $A_1 = 2N(W_c + H_c)L_x = 2(1 + \alpha)\beta L_z L_x$; A_2 is the heat conduction area, as a significant amount of heat is conducted along the height direction of the heat sink by the ribs; A_2 can be adopted as the base area of the ribs or $A_2 = N W_r L_x = (1 - \beta)L_z L_x$; and L is mean heat conduction path, which is assumed as heat sink height or $L = L_y$ (see Fig. 4).

Data in Fig. 3(a) are taken as an example in determining the effect of number of channels, N , on optimal thermal resistance with $\alpha = 10$ and $\beta = 6$. The minimum number of channels considered is 50, since turbulent flow will occur with fewer channels, thereby deviating from the assumption adopted for the proposed model [13]. As N increases, $W_c + H_c = L_z/N$ decreases. When $\beta = W_c/(W_c + W_r)$ is fixed, both W_c and W_r decrease accordingly. Since $\alpha = H_c/W_c$ is fixed, H_c also decreases, causing $L = L_y = \delta_1 + H_c + \delta_2 = H_c + 200 \mu\text{m}$ to decrease. From Eq. (9a), as N increases, u_m decreases, which reduces h . From Eq. (19), increasing N increases convective thermal resistance and reduces conductive thermal resistance. Thus, the optimal thermal resistance depends on competition between these two thermal resistances in Eq. (19). Under the condition of $50 < N < 63$ with $\alpha = 10$ and $\beta = 6$, u_m is high (0.957 m s^{-1} for $N = 50$ and 0.853 m s^{-1} for $N = 63$) (Fig. 5), producing efficient convective heat transfer. The solid material is a silicon wafer, which has a high thermal conductivity; thus, both convective thermal resistance and conductive thermal resistance are low, leading to low overall thermal resistance under optimal conditions. Notably, optimal thermal resistance decreases slightly as N increases (0.142 K W^{-1} for $N = 50$ and 0.138 K W^{-1} for $N = 63$). At $N > 63$, as N increases, both u_m and h decrease (0.827 m s^{-1} for $N = 67$, 0.524 m s^{-1} for $N = 167$), such that convective thermal resistance is predominant (although conductive thermal resistance still decreases as N decreases). The net effect is that optimal thermal resistance increases rapidly as N increases (0.138 K W^{-1} for $N = 67$ and 0.249 K W^{-1} for $N = 167$).

With $N = 100$ and $\alpha = 10$, the optimal thermal resistance first decreases and then increases with an optimal value of $\beta = 0.68$ (Fig. 3(b)). The same tendency exists for $\beta = 0.6$, giving optimal values of $\alpha = 19$ with $N = 100$ (Fig. 3(c)). Li and Peterson [25] and Weisberg et al. [10] demonstrated that optimal thermal resistance decreases monotonously as α increases. This difference in observations by Li and Peterson [25] and Weisberg et al. [10] with ours reported herein is attributable to the fact that these the former two studies limited α to <6.

Based on the above analyses, optimal thermal resistance for a heat sink with the specified solid material and coolant mainly de-

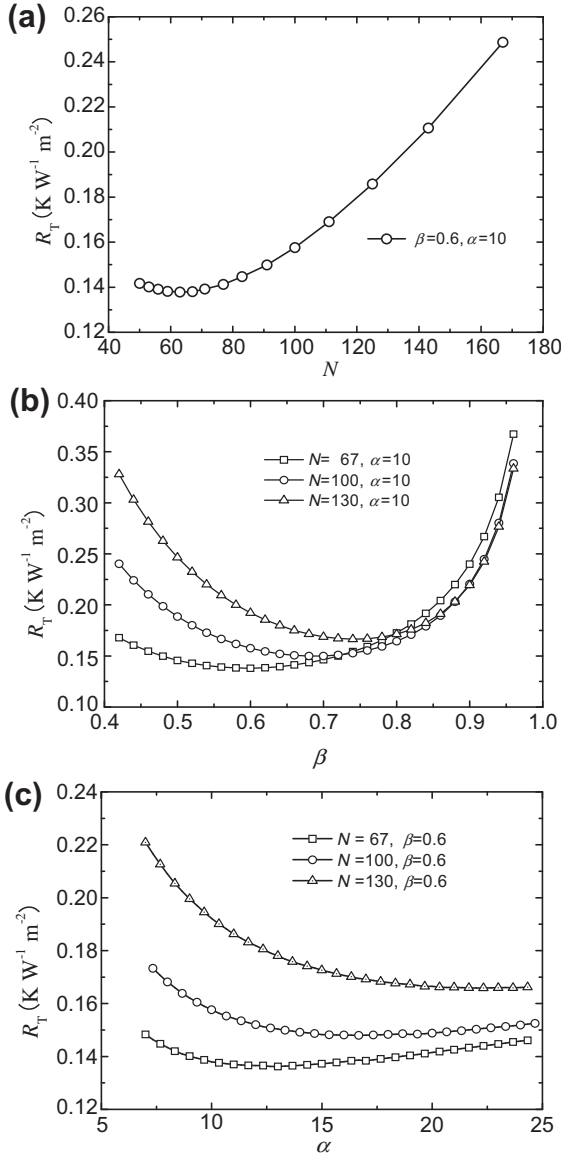


Fig. 3. The effect of individual parameter on optimal thermal resistance: (a) channel number, N ; (b) width ratio of channel to pitch, β and (c) aspect ratio of channel, α .

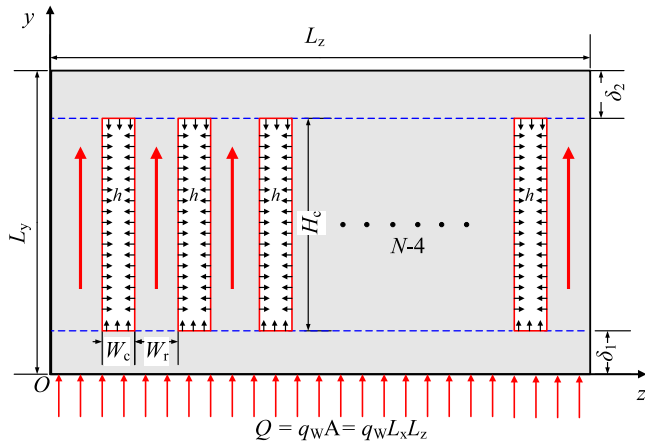


Fig. 4. The sketch of heat transfer in the microchannel heat sink.

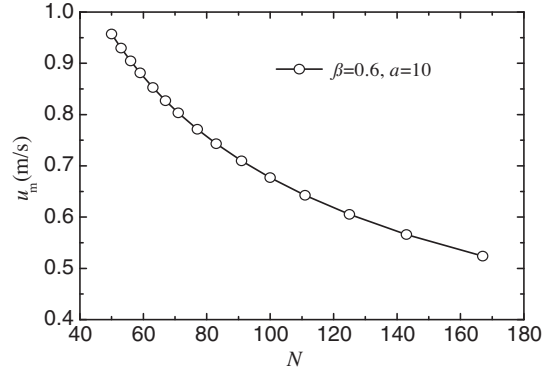


Fig. 5. The effect of the channel number on average flow velocity of coolant over the channel cross-section.

depends on h, A_1, A_2 , and L . With a constant heat flux, q_w , and pumping power, Ω , as constraints, any change in N, α , or β causes corresponding changes to h, A_1, A_2 , and L ; thus, convective and conductive thermal resistance and optimal thermal resistance vary. Therefore, the next section simultaneously optimizes N, α , and β .

4.3. Heat sink optimization

When $L_x = L_z = 10 \text{ mm}$, $L_y = 900 \mu\text{m}$, $\delta_1 = 100 \mu\text{m}$, and $\delta_2 \geq 100 \mu\text{m}$, $H_c \leq 700 \mu\text{m}$. The coolant inlet temperature and pumping power are $T_{in} = 293 \text{ K}$ and $\Omega = 0.05 \text{ W}$, respectively, and heat flux is $q_w = 100 \text{ W cm}^{-2}$.

Fig. 6 shows the convergence trajectory for N, β , and α with three sets of initial guesses ($N = 125, \alpha = 12.5$, and $\beta = 0.4$; $N = 56, \alpha = 4.8$, and $\beta = 0.4$; and $N = 63, \beta = 3.9$, and $\beta = 0.8$) in optimization calculations. The same optimal point is obtained using these three initial guesses. This finding confirms that the obtained optimal design is at least a local optimal solution for the objective function $J = R_T$. The optimal values for the geometrical parameters are $N = 71, \alpha = 8.24$ and $\beta = 0.60$, with a corresponding thermal resistance of $R_T = 0.144 \text{ K W}^{-1}$ (Fig. 7).

Fig. 8(a) and (b) shows coolant velocities along the channel centerline and along the channel width at various search steps, respectively, from the first initial guess of $N = 125, \alpha = 12.5$, and $\beta = 0.40$. During search step 1, the coolant velocity along the channel center-

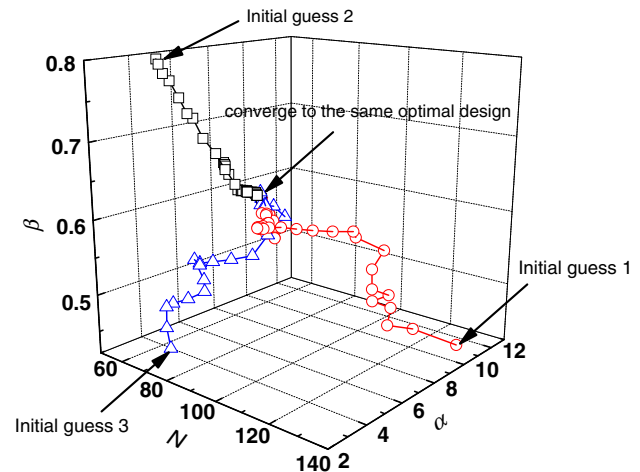


Fig. 6. Change in N, α and β during optimization for three initial guesses. Initial guess 1: $N = 125, \alpha = 12.5$ and $\beta = 0.4$; initial guess 2: $N = 56, \alpha = 4.8$ and $\beta = 0.4$; initial guess 3: $N = 63, \alpha = 3.9$ and $\beta = 0.8$.

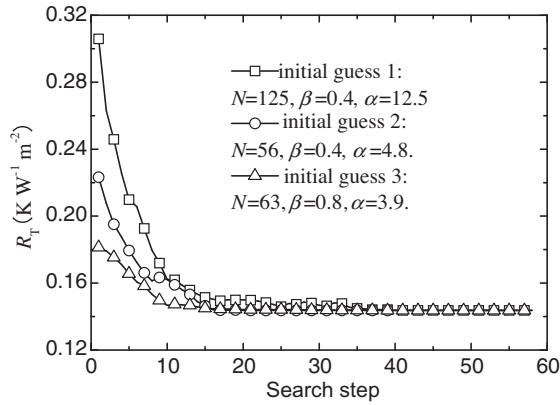


Fig. 7. Change in optimal thermal resistance during optimization for various initial guesses.

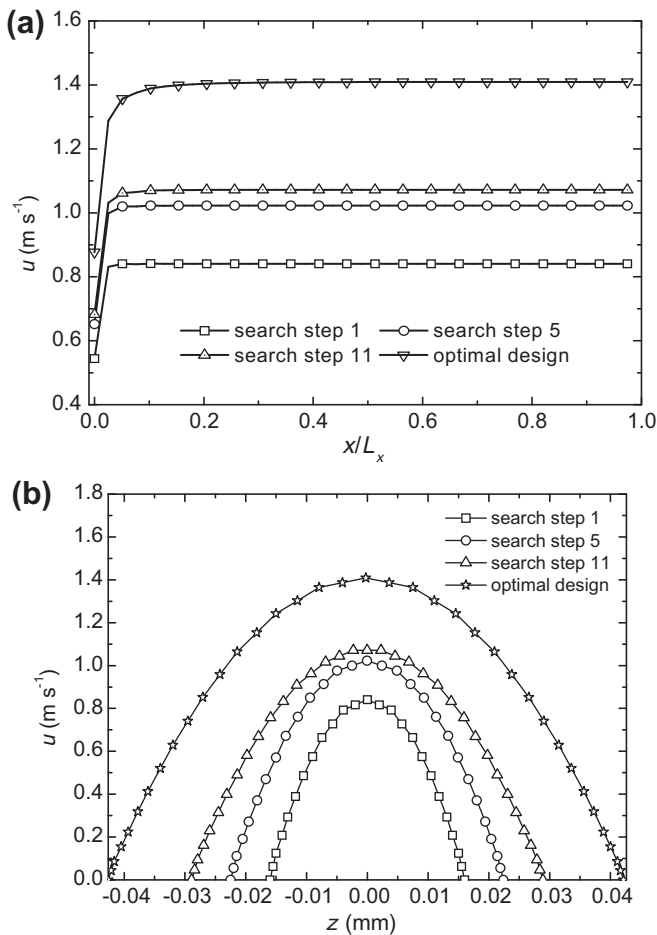


Fig. 8. Coolant velocity at various search steps: (a) along channel width and (b) along channel centerline.

line is low (0.841 m s^{-1} for fully developed velocity) when $N (=125)$ is excessively large and β (0.40) is small. During search step 5, the fully developed velocity increases to 1.02 m s^{-1} when N is reduced to 102 and β is increased to 0.46. During search step 11, the fully developed velocity increases to 1.07 m s^{-1} with $N = 96$ and $\beta = 0.56$. The centerline velocity further increases to 1.409 m s^{-1} in the final optimal solution.

Fig. 9 shows the temperature distribution in the solid and fluid regions along y - z middle cross section of the channel during vari-

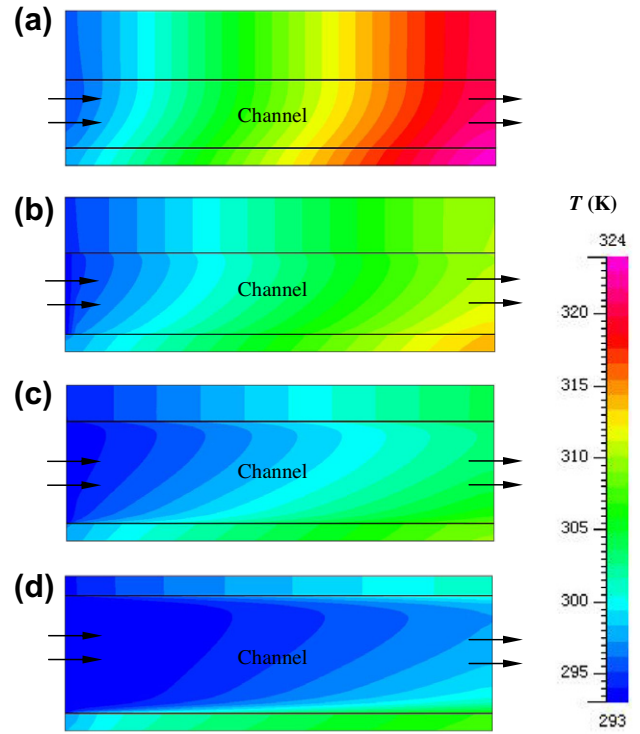


Fig. 9. Temperature distribution in solid and fluid regions along y - z middle cross-section of channel at various search steps:(a) search step 1; (b) search step 5; (c) search step 11 and (d) optimal design.

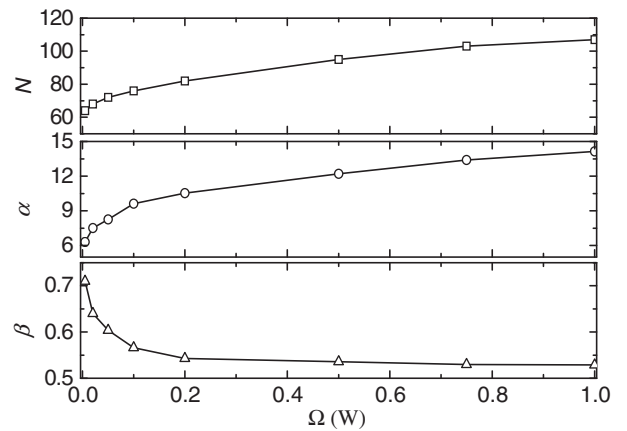


Fig. 10. Optimal geometric parameters for various pumping powers.

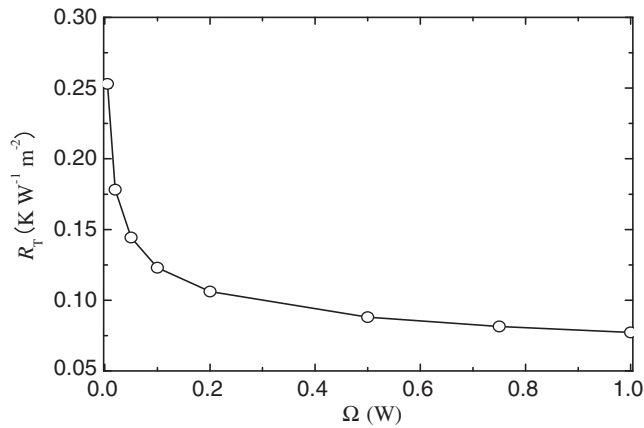
ous search steps. The maximum solid temperature occurs at the bottom outlet. Solid temperature decreases when coolant velocity increases during optimization steps. For instance, maximum solid temperature is 323.6 K in step 1, and then decreases to 314.0 K in search step 5; this continues until 307.4 K is reached in the final optimal solution. The uniformity of the coolant temperature distribution increases as the search process proceeds.

The above optimal geometrical parameters are limited under $\Omega = 0.05 \text{ W}$. Figs. 10 and 11 show the effects of pumping power on the corresponding optimal geometrical parameters. As pumping power increases, the optimal number of channels, N , and optimal channel aspect ratio, α , increases, and the optimal ratio of the channel width to pitch, β , decreases (Fig. 10). Based on the study of individual parameters (Fig. 3(c)), α increases to 12 at $\beta = 0.6$, thereby reducing optimal thermal resistance. Since channel height,

Table 2

The inlet velocity for optimal design at various pumping powers.

Ω (W)	0.005	0.02	0.03	0.05	0.10	0.20	0.50	0.75	1.00
u_m (m s ⁻¹)	0.332	0.610	0.723	0.885	1.098	1.464	2.057	2.262	2.482

**Fig. 11.** Minimum optimal thermal resistance for various pumping powers.

H_c , cannot exceed 700 μm in this study, the optimal design increases N to decrease channel width and then increase α . The decreased β increases heat conduction area, A_2 , which reduces conductive thermal resistance. Although increasing N and α reduces inlet flow velocity, pumping power, Ω , also increases, thereby compensating for the reduced inlet flow velocity (Eq. (9a)). Inlet velocity still increases as pumping power increases (Table 2).

Fig. 11 shows the minimum optimal thermal resistances at various pumping powers, Ω . As Ω increases, optimal thermal resistance reduces gradually. However, the reduction rate in the optimal thermal resistance for a high Ω is much less than that for a low Ω . For instance, optimal thermal resistance decreases from 0.253 K W^{-1} at $\Omega = 0.005$ W to 0.123 K W^{-1} at $\Omega = 0.10$ W, and decreases from 0.106 K W^{-1} at $\Omega = 0.20$ W to 0.077 K W^{-1} at $\Omega = 1.00$ W, meaning that the increase in pumping power is not always effective in practical designs.

5. Conclusions

This work optimizes design parameters of a microchannel heat sink using a novel inverse problem solution method composed of a simplified conjugate-gradient method (inverse problem solver) and a full three-dimensional heat transfer and flow model (direct problem solver). With constant A (10 mm \times 10 mm), q_w (100 W cm^{-2}), and Ω as constraints, three design parameters—number of channels, N , channel aspect ratio, α , and ratio of channel width to pitch, β , are simultaneously optimized to obtain minimum overall thermal resistance. When $\Omega = 0.05$ W, the optimal design with $N = 71$, $\beta = 0.6$ and $\alpha = 8.24$ is achieved, giving a corresponding optimal thermal resistance of 0.144 K W^{-1} . The optimal thermal resistance decreases as pumping power increases. However, the reduction rate in optimal thermal resistance declines under high pumping powers, suggesting that increasing pumping power is not always cost-effective for practical heat sink designs.

Acknowledgments

This study was supported by the National Natural Science Foundation of China (Nos. 51076009, U1034004, and 50825603). In addition, the financial support by the National Science Council

through the Contract NSC99-2212-E211-010-MY2 was acknowledged.

References

- [1] D.B. Tuckerman, R.F.W. Pease, High-performance heat sinking for VLSI, *IEEE Electr. Dev. Lett.* EDL-2 (1981) 126–129.
- [2] J. Li, G.P. Peterson, P. Cheng, Three-dimensional analysis of heat transfer in a micro heat sink with single phase flow, *Int. J. Heat Mass Transfer* 47 (2004) 4215–4231.
- [3] J.H. Ryu, D.H. Choi, S.J. Kim, Numerical optimization of the thermal performance of a microchannel heat sink, *Int. J. Heat Mass Transfer* 45 (2002) 2823–2827.
- [4] C.W. Chen, J.J. Lee, H.S. Kou, Optimal thermal design of microchannel heat sinks by the simulated annealing method, *Int. Commun. Heat Mass Transfer* 35 (2008) 980–984.
- [5] R. Chein, J. Chen, Numerical study of the inlet/outlet arrangement effect on microchannel heat sink performance, *Int. J. Therm. Sci.* 48 (2009) 1627–1638.
- [6] K. Kawano, K. Minakami, H. Iwasaki, M. Ishizuka, Development of micro channels heat exchanging, in: R.A. Nelson Jr., L.W. Swanson, M.V.A. Bianchi, C. Camci (Eds.), *Application of Heat Transfer in Equipment, Systems, and Education*, HTD-vol. 361-3/PID-vol. 3, ASME, New York, 1998, pp. 173–180.
- [7] W. Qu, I. Mudawar, Experimental and numerical study of pressure drop and heat transfer in a single-phase micro-channel heat sink, *Int. J. Heat Mass Transfer* 45 (2002) 2549–2565.
- [8] I. Tiselj, G. Hetsroni, B. Mavko, A. Mosyak, E. Pogrebnyak, Z. Segal, Effect of axial conduction on the heat transfer in microchannels, *Int. J. Heat Mass Transfer* 47 (2004) 2551–2565.
- [9] P. Lee, S.V. Garimella, D. Liu, Investigation of heat transfer in rectangular microchannels, *Int. J. Heat Mass Transfer* 48 (2005) 1688–1704.
- [10] A. Weisberg, H.H. Bau, J.N. Zemel, Analysis of micro channels for intergrated cooling, *Int. J. Heat Mass Transfer* 35 (1992) 2465–2474.
- [11] L.T. Hwang, I. Turlik, A. Reisman, A thermal module design for advancing packaging, *J. Electr. Mater.* 16 (1987) 347–355.
- [12] R.W. Knight, J.S. Goodling, D.J. Hall, Optimal thermal design of forced convection heat sinks – analytical, *J. Electron. Packag.* 113 (1991) 313–321.
- [13] R.W. Knight, D.J. Hall, J.S. Goodling, R.C. Jaeger, Heat sink optimization with application to micro channels, *IEEE Trans. Comp. Hybrids Manuf. Technol.* 15 (1992) 832–842.
- [14] Z. Wen, K.F. Choo, The optimum thermal design of microchannel heat sinks, in: *IEEE/CPMT Electronic Packaging Technology Conference*, 1997, pp. 123–129.
- [15] A.G. Fedorov, R. Viskanta, Three-dimensional conjugate heat transfer in the microchannel heat sink for electronic packaging, *Int. J. Heat Mass Transfer* 43 (2000) 399–415.
- [16] W. Qu, I. Mudawar, Analysis of three-dimensional heat transfer in micro-channel heat sinks, *Int. J. Heat Mass Transfer* 45 (2002) 3973–3985.
- [17] G. Gamrat, M. Favre-Marinet, D. Asendrych, Conduction and entrance effects on laminar liquid flow and heat transfer in rectangular microchannels, *Int. J. Heat Mass Transfer* 48 (2005) 2943–2954.
- [18] J.L. Xu, Y.H. Gan, D.C. Zhang, X.H. Li, Microscale heat transfer enhancement using thermal boundary redeveloping concept, *Int. J. Heat Mass Transfer* 48 (2005) 1662–1674.
- [19] G.L. Morini, Laminar forced convection of liquid flows through silicon microchannels, *J. Fluid. Eng.* 126 (2004) 485–489.
- [20] G.L. Morini, M. Spiga, The role of the viscous dissipation in heated microchannels, *J. Heat Transfer* 129 (2007) 308–318.
- [21] J.T. Liu, X.F. Peng, W.M. Yan, Numerical study of fluid flow and heat transfer in microchannel cooling passages, *Int. J. Heat Mass Transfer* 50 (2007) 1855–1864.
- [22] Z. Li, X. Huai, Y. Tao, H. Chen, Effects of thermal property variations on the liquid flow and heat transfer in microchannel heat sinks, *Appl. Therm. Eng.* 27 (2007) 2803–2814.
- [23] S.J. Kim, Method for thermal optimization of microchannel heat sinks, *Heat Transfer Eng.* 25 (2004) 37–49.
- [24] K.K. Ambatipudi, M.M. Rahman, Analysis of conjugate heat transfer in microchannel heat sinks, *Numer. Heat Transfer* 37 (2000) 711–731.
- [25] J. Li, G.P. Peterson, Geometric optimization of a micro heat sink with liquid flow, *IEEE Trans. Comp. Packag. Technol.* 29 (1) (2006) 145–154.
- [26] J. Li, G.P. Peterson, 3-Dimensional numerical optimization of silicon-base high performance parallel microchannel heat sink with liquid flow, *Int. J. Heat Mass Transfer* 50 (2007) 2895–2904.
- [27] T. Bello-Ochende, L. Liebenberg, J.P. Meyer, Constructal cooling channels for microchannel heat sinks, *Int. J. Heat Mass Transfer* 50 (2007) 4141–4150.
- [28] H.S. Kou, J.J. Lee, C.W. Chen, Optimum thermal performance of microchannel heat sink by adjusting channel width and height, *Int. Commun. Heat Mass Transfer* 35 (2008) 577–582.

- [29] K.C. Toh, X.Y. Chen, J.C. Chai, Numerical computation of fluid flow and heat transfer in micro channels, *Int. J. Heat Mass Transfer* 45 (2002) 5133–5141.
- [30] H. Al-Bakhit, A. Fakheri, Numerical simulation of heat transfer in simultaneously developing flows in parallel rectangular ducts, *Appl. Therm. Eng.* 26 (2006) 596–603.
- [31] X.D. Wang, Y.X. Huang, C.H. Cheng, J.Y. Jang, D.J. Lee, W.M. Yan, A. Su, An inverse geometry design problem for optimization of single serpentine flow field of PEM fuel cell, *Int. J. Hydrogen Energy* 35 (2010) 4247–4257.